Enviado para publicar por Elsevier: Fuel 83 (2004) 1733–1742

Effect of pore geometry on the sintering of Ca-based sorbents during calcination at high temperatures

J. Adánez*, V. Fierro†, F. García-Labiano

Instituto de Carboquímica (C.S.I.C.), Department of Energy and Environment

Miguel Luesma Castan 4, 50015 Zaragoza, Spain

Abstract

In this paper, we present a mathematical model that describes the calcination and sintering of calcium-based sorbents in furnace sorbent injection (FSI) conditions. We assumed that the sorbent decomposition follows a shrinking core model with a changing pore size distribution in every layer and we used a comprehensive mathematical model for sintering. Cylindrical and plate-like or slit pore geometries, usually associated with carbonate- and hydroxide-derived sorbents, respectively, were adopted and compared. It was concluded that sorbents with cylindrical pores sinter to a grater extent than those with slit pores. The decomposition and sintering kinetics were determined for three calcium sorbents with different pore geometries in FSI conditions. The study revealed that the presence of CO_2 and H_2O in the reaction atmosphere affects the sintering parameters whereas the calcination parameters remain constant. The model effectively correlated the experimental data and adequately predicted not only the evolution of the specific surface area but also the evolution of the pore size distribution of the sorbent over time. The most striking aspect of the research was that although our model calculated the total area by adding together the pore sizes in all the layers of the sorbent, the results were very similar to those of other sintering models.

* Corresponding author. Tel.: 34-976733977; Fax: 34-976733318; *E-mail address*: jadanez@carbon.icb.csic.es (J. Adánez)

† Present address: Departament d'Enginyeria Quimica. Escola Tècnica Superior d'Enginyeria Química. Universitat Rovira i Virgili. Campus Sescelades 43007, Tarragona, Spain. E-mail: vfierro@etseq.urv.es

Keywords: Sintering model, Furnace sorbent injection, Calcium-based sorbent, Pore geometry

1. Introduction

Limestones and calcium hydroxides are calcium-based sorbents that are usually used as SO_2 removal agents. One of the most widely used technologies is sorbent injection into pulverised coal boilers, which is specially attractive as the lowest cost option to retrofit old power plants that burn coal with a low sulphur content [1]. Temperatures in the furnace are high and a suitable thermal window for the reaction lies approximately between 900 and 1200 °C. The residence time for the combustion gas, and hence for the entrained sorbent particles within the thermal window, depends on the type of boiler, but in most cases it is less than 1.5 s. The sorbent particle is small, typically less than 50 μm, and the capture of SO_2 is enhanced by smaller particles. When a calcium-based sorbent, a calcium carbonate or a hydroxide is injected at high temperatures it decomposes to form a porous solid, CaO:

$$CaCO_3 \rightleftharpoons CaO + CO_2$$

$$Ca(OH)_2 \rightleftharpoons CaO + H_2O$$

Beruto et al. [2] found that the porous structure of CaO depended on the parent material, $CaCO_3$ (c-CaO) or $Ca(OH)_2$ (h-CaO). Nitrogen adsorption-desorption isotherms of the c-CaO and h-CaO have normally been associated with cylindrical or plate-like pores, respectively [3]. However, some limestones can also show slit pores [4,5].

SO_2 removal depends on the structural characteristics, porosity and specific surface area of the sorbent that develop during calcination and which are modified by sintering [6-8]. Of the factors affecting the sintering process, the most important are sorbent impurities [9] and, above all, the presence of such gases as CO_2 and H_2O in the combustion process [10]. Several models in the literature show the dependence of the sintering rate on the CO_2 and H_2O concentrations [11-15]. However, most of them suffer from the lack of a pore size distribution, which can have a considerable effect on the sulphation predictions and the values of the kinetic parameters [2, 16, 17].

Moreover, none of the previous models considers the pore structure differences between the calcined products, c-CaO and h-CaO, which can have an important effect on the sintering process during calcination.

Although studies have been made of calcination/sintering kinetics carried out with sorbents in fluidised bed reactors or in flue gas desulphurisation systems [18-19], the fact that the conditions are very different from those in FSI systems means that they cannot be used to predict sorbent behaviour during injection. Additionally, the experimental problems associated with the thermogravimetric measurements of the $CaCO_3$ decomposition of small particles have been widely shown [20]. Therefore, to adequately characterise the sorbent behaviour of a small sorbent, at high temperature and for short times, a differential reactor [20] or an entrained flow reactor [12, 21-23] must be used.

The aims of this paper were (i) to study the simultaneous calcination-sintering processes of different calcium-based sorbents in a drop tube reactor to simulate as closely as possible the conditions in typical FSI systems; (ii) to predict the evolution of the pore size distribution, for cylindrical and plate-like pore geometries, in different operation conditions by developing a decomposition-sintering model for cylindrical and plate-like geometries.

2. Experimental

2.1. Apparatus

The calcination/sintering experiments were carried out in a drop tube reactor system at temperatures between 900 and 1200°C and residence times varying from 0.25 to 1.2s. To test the effect of the gases on solid sintering, atmospheres with variable percentages of CO_2 (0-15%), H_2O (0-7%) and nitrogen balance were used. More details on the experimental set up are given elsewhere [17].

The calcination degree was determined by the weight loss in a thermobalance at 900 ºC in nitrogen. Specific surface areas and pore size distributions of the calcines were determined by nitrogen physisorption at 77 K in an ASAP 2000 analyser.

2.2. Sorbents

Three calcium-based sorbents were used here: the Omyacarb limestone and two calcium hydroxides prepared from it, CH-45 and CH-LGS [5]. CH-45 was prepared by calcining Omyacarb limestone and further hydration. CH-LGS was prepared by adding calcium lignosulfonate (LGS) to the hydrating water to get a percentage of 1.5 wt% in the dried product [17]. The main physical properties of these three raw sorbents are shown in Table 1. Both calcium hydroxides have higher specific surface areas than the limestone because of the consolidated nature of this material. The particle size of CH-LGS is somewhat smaller than that of CH-45, because of the dispersing properties of the LGS. The adsorption-desorption isotherms of the Omyacarb limestone correspond to a type H1 hysteresis loop (IUPAC classification), while the calcium hydroxides showed a type H3 hysteresis loop at all the temperatures tested. According to Gullet and Bruce [3], type H1 hysteresis loops are generally associated with cylindrical pores while type H3 are associated with slit-shaped or parallel plate-like pores. In this study, we used the BJH model [24] to obtain the pore size distribution for the sorbent samples with cylindrical pores and the model proposed by Innes [25] for the calcium hydroxides with plate-like pore geometry.

3. Calcination-sintering model

3.1. Previous models

Thermal decomposition of a calcium-based sorbent involves several potential rate-controlling processes: heat transfer to the surface and through the CaO product layer, mass transfer of CO_2 through the product layer and the decomposition reaction itself. Powell and Searcy [26] said that heat and mass transfer were not limiting for small, dispersed particles. Borgwardt [20] agreed that the calcination process of small particles (1-90 μm) was under chemical kinetic control, and added that the calcination

rate was proportional to the BET surface area. Silcox et al. [15] developed a mathematical model for the flash calcination of $Ca(OH)_2$ and $CaCO_3$ particles described by the shrinking core model. In this model, the particle was assumed to be isothermal although internal CO_2 profiles were considered. Ghosh-Dastidar et al. [22] also used this type of model to describe the calcination of very small (<5 μm) $Ca(OH)_2$ particles. On the other hand, Hu and Scaroni [27] considered calcination to occur throughout the particle with different degrees of calcination at different locations.

Calcination is a fast reaction that initially yields a very high surface area of the CaO produced, which rapidly decreases as the sintering progresses [9]. Most of the previous studies made extremely simplified assumptions about the phenomena involved; namely, the simultaneous occurrence of calcination and sintering. Previous FSI modelling efforts [7, 28] assumed that calcination was instantaneous or experimentally excluded this effect by using precalcines. Silcox et al. [15] proposed perhaps the most thorough FSI model to date, describing the decomposition at the reactant-product interface, the diffusion of CO_2 or H_2O through the CaO layer, and the sintering of the CaO layer. However, the calcium hydroxide was assumed to dehydrate almost instantaneously and so it was not considered in the model. Although they included sintering effects, the model suffered from the lack of knowledge of the pore size distribution and how it varied over time.

As mentioned above, the sintering process modifies the pore structure developed in the sorbent during calcination. Different mathematical expressions have been reported to predict the surface area as a function of time during the calcination-sintering process. The German-Munir model [13], based on the neck-growth models, can be expressed by

$$\left(\frac{S_0 - S}{S_0}\right)^{\gamma} = k_s\, t \qquad \text{for } \Delta S/S_0<50\% \qquad (1)$$

Sintering effects on precalcines have been described as proportional to the difference between the specific surface area and an asymptotic surface area, S_f,

$$\frac{dS}{dt} = -k_s \left(S - S_f\right)^n \quad (2)$$

Different kinetic orders have been suggested for this equation. Nicholson [29] reported a first-order kinetic, while Bortz et al. [30], Borgwardt [9] and Mai [11] reported a second order for the calcium oxide sintering. Borgwardt [9] used an asymptotic surface area of 5 m^2 g^{-1} and Mai [12] used an asymptotic surface area of 20.2 m^2 g^{-1} for the sintering of CaO from calcium hydroxide.

Fuertes et al. [31] deduced an expression, based on the German-Munir model, to fit the variation in the specific surface area with time for particles about 1 mm.

$$S = S_0 - \left(S_0 - S_f\right)\left[1 + k_s t\left(\frac{S_0}{S_0 - S_f}\right)^{\gamma}\right]^{1/\gamma} \quad (3)$$

On the other hand, Irabien et al. [18] used the German and Munir model [13] to correlate their experimental results when $\Delta S/S_0<55\%$, and an empirical model when the surface area is directly proportional to the heating time for a surface reduction higher than 55%.

Some of the above equations have also been modified to take into account the influence of H_2O and CO_2 on the sintering process [14, 22]. However, they all consider only the surface evolution of the sorbent and disregard the pore size distribution, which also plays an important role in sulphation [32, 33]. Moreover, with these equations, it is not possible to study how the pore geometry, which is of considerable importance during sulphation, affects the sintering process [17].

3.2. Model description

3.2.1. Calcination model

The sorbent decomposition was modelled with the shrinking core model developed by Silcox et al. [15], who proposed that the process was controlled by the chemical reaction and the gas diffusion (CO_2 or H_2O) through the CaO formed. The particle is assumed to be isothermal and the decomposition process is allowed to occur

in steps, which leads to a layered CaO zone with different physical properties in each layer.

The equations governing the movement of the calcination front were

$$\frac{dR}{dt} = -\frac{M}{\rho} k_c \qquad P<10^{-2} P_e \qquad (4)$$

$$\frac{dR}{dt} = -\frac{M}{\rho} k_c \frac{(P_e - P)}{P_e} \qquad 10^{-2} P_e<P<P_e \qquad (5)$$

These expressions are based on data from Darroudi and Searcy [34], who demonstrated a two-region CO_2 pressure effect. The equations used to calculate the equilibrium pressure were the ones proposed by Weast [35] for CO_2 and by Matsuda et al. [36] for H_2O.

The differential equation governing the diffusion of CO_2 or H_2O through the porous lime is

$$\frac{\partial^2 P}{\partial R^2} + \left(\frac{2}{R} + \frac{1}{De}\frac{\partial De}{\partial R}\right)\frac{\partial P}{\partial R} = \frac{1}{De}\frac{\partial P}{\partial t} \qquad (6)$$

with the following boundary conditions

at $R=R_p$, $$-De \frac{\partial P}{\partial R} = k_g (P - P_b) \qquad (7)$$

at $R=R$, $$-\frac{De}{R_g T}\frac{\partial P}{\partial R} = k_c \frac{(P_e - P)}{P_e} \qquad (8)$$

The external mass-transfer coefficient, kg, was calculated by using a Sherwood number of 2. The effective diffusivity, De_K, in every layer K, was calculated as a function of the Knudsen and molecular diffusions, and the sorbent porosity in the layer, [37]

$$De_K = \left(\frac{1}{\overline{D_K}} + \frac{1}{D_A}\right)_K^{-1} \varepsilon_K^2 \qquad (9)$$

The molecular diffusion was calculated by the expression of Fuller et al. [38]. An average Knudsen diffusion coefficient ($\overline{D_K}$) was used that took into account the pore size distribution for every layer of CaO formed,

$$\overline{D_K} = \sum_{i=1}^{n} D_{K_i} fv_{K,i} = \sum_{i=1}^{n} \left(97 r_i \sqrt{\frac{T}{M}} \right) fv_{K,i} \quad (10)$$

3.2.2. Sintering model

During sorbent injection, a new surface area is generated by calcination and quickly reduced by sintering. The simultaneous effect of these processes produces an internal surface area that greatly affects the use of the sorbent during the subsequent SO_2 removal process. This study used a sintering model corresponding to the two different pore geometries of CaO (cylinders and slits). Sintering reduces the surface area because the pores coalesce, but its effect on pore volume is negligible [3] and the particle size remains constant [31]. We assumed that the nascent CaO surface area and pores depend on the nature of the calcium sorbent and that the sintering process proceeds by the coalescence of two pores to form one, while the total pore volume remains constant. Figure 1 shows a scheme of the sintering process for the two pore geometries considered (cylinders and slits). For the cylindrical pore geometry, the characteristic dimension is the pore radius r_i, while for a system of parallel plates it is the distance from the pore wall to the centre z_i. Because the pore geometries were different, they were analysed separately. Table 2 shows the equations that were used. For the cylindrical pore geometry, the radius of the new pore r_{ij} that formed from the coalescence of pores r_i and r_j is calculated assuming that they were of the same length, $L_i = L_j$. For the plate-like pore geometry, we assumed that all the pores had the same surface area, $Sp_i = Sp_j$, but that the number of pores of every size $n_i \neq n_j$ was different. As the number of pores cannot be determined separately, two new parameters, φ_{ij} and Ω_{ij}, were introduced for cylindrical and plate-like pores, respectively.

When a layer of $CaCO_3$ or $Ca(OH)_2$ decomposes, a new surface of CaO is generated. Thus, every layer K has an initial surface area before sintering $S_{0K.}$ The initial pore size distribution for cylindrical pores $\varphi_{0K,i}$ is calculated using the method of Barret et al. [24] as a function of the initial specific surface area in the CaO ($S_{0K,i}$) and the radius r_i where the surface is generated,

$$\varphi_{0K,i} = \frac{S_{0K,i}}{2\pi\ r_i} \qquad (11)$$

A similar equation is obtained for plate-like pores although in this case it is necessary to use the method proposed by Innes [25] to analyse the nitrogen physisorption data. The sintering of these initial pores of calcined sorbent depends on the operational conditions. In order to calculate the specific surface area of a partially calcined particle, the surfaces of every layer, S_K, must be added together. The specific surface area of a calcined layer is the result of integrating the pore areas for all the pore sizes in the layer K. The calculation of the overall specific surface area, S, takes into account the weight fraction of every layer in the particle and the weight fraction of the unreacted core together with their corresponding specific surface areas,

$$S = \sum_{i=1}^{n} S_K fw_K + S_{sorb} fw_{sorb} \qquad (12)$$

To adequately plot the pore size distributions measured, we used the ratio:

$$g(dp) = \frac{S_i}{\Delta\ dp_i} \qquad (13)$$

where dp_i is the characteristic distance of either the cylindrical geometry (diameter) or the plate-like geometry (distance between surfaces).

3.2.5. Solution procedure

The decomposition of carbonate or hydrate particles was modelled by the shrinking-core model, which considers that a calcined shell is produced as the reaction interface recedes. A new shell is then calcined and, simultaneously, the previous calcined shell undergoes sintering, and so on. The process can be described as the formation of a multilayered CaO shell, each layer corresponding to CaO of a different age.

The decomposition reaction takes place at the $Ca(OH)_2$ or $CaCO_3$ /CaO interface. The model simulates the build up of H_2O or CO_2 partial pressure at the reaction

interface and the profiles of CO_2/H_2O pressure along the radius of the particle and their evolution with time. These profiles depend on the decomposition rate and the diffusional resistance inside the particle, which is determined by the porous system developed during calcination and modified by sintering.

The concentration profiles of CO_2 or H_2O were calculated using the numerical solution proposed by Silcox et al. [15] and D_K as defined in Eq. (10). This coefficient varies with time because of the changes produced in the pore size distribution of every calcined layer by sintering.

In the model, the sintering process takes place simultaneously with the sorbent decomposition in those zones where the sorbent is already calcined. Each calcined layer has a different sintering time, specific surface area and pore size distribution. The most recently formed layer of CaO has the highest surface, which corresponds to the nascent CaO. The sintering process modifies the pore structure of the nascent CaO. The sintering submodel is applied to each layer in each period of time, taking into account the pore geometry of the sorbent considered. The specific surface area and pore size distribution of the whole particle is finally calculated by integrating the different pore sizes in all the layers of the sorbent, even those of the raw sorbent where the calcination has still not taken place.

4. Results and discussion

The combined calcination and sintering model developed makes it possible to predict the evolution of the internal structure of the sorbent at different locations, and its evolution over time. If the calcination of the sorbent particles follows a shrinking core model, the external shells are sintered while the inner part of the particle is still being calcined. Thus, the radial profiles of the specific surface area throughout the particle are continuously varying, as shown in Fig. 2a. The specific surface area of the external zone is lower than that of the layer just calcined because it has undergone a longer, more severe sintering, and the values of the profiles decrease from 104 $m^2\ g^{-1}$ to about 40 $m^2\ g^{-1}$. These values are lower if the particle is maintained at high temperatures after

calcination has been completed. Moreover, each zone has a different pore size distribution, as can be observed in Fig. 2b at τ=1. Curve C corresponds to the pore size distribution of the nascent CaO and curve A to the external shell, the first one calcined and, therefore, the one that is most sintered. As indicated above, the initial small pores are sintered and disappear to form bigger pores, as a result of which the pore size distribution shifts to larger pore sizes as sintering occurs. In this way, the external shells have a widespread pore size distribution bigger pores than the internal shells where nascent CaO is present.

4.1. Effect of the pore shape

c-CaO and h-CaO have been associated with cylindrical or plate-like pores, respectively [3], but some limestones can also show slit pores as found by Adánez et al. [17] and Fierro [39]. Differences in the pore structure of the calcined products can have an important effect on the sintering process during calcination and further sorbent use during injection.

In order to study the effect of the pore shape on the sintering process, we used a particle diameter of 50 μm and a nascent specific surface area of 104 m^2g^{-1} generated in a pore with a characteristic distance of 4nm (pore radius or distance between plates). The simulation was carried out at a temperature of 1273 K with the same rate constant for the decomposition of the sorbent (k_c= 10^{-1} mol m^{-2} s^{-1}). For the two geometries considered in this work, the driving force for the sintering was the parameter φ, for cylindrical pores, and Ω, for plate-like pores. Because the equations that define the sintering process for each geometry are different, the values of the sintering constants are also very different from each other. This makes it difficult to directly compare the effect of the pore geometry with the same value of the sintering constant. So, a sintering constant that decreases the specific surface area by 5% in 2 s was adopted as a reference basis for each of the two geometries considered. The sintering constant taken as a reference for cylindrical pores was $K_s^*{}_{cil}$ =10^{-10} g m^{-1} s^{-1} and for plate-like pores it was $K_s^*{}_{plate}$ =10^{-4} g m^{-2} s^{-1}. A new parameter β was used to detect the effect of the

pore geometry on sintering. This new parameter is a multiplier of the basic sintering constants defined above.

$$K_{s\,cil} = \beta \; K^{*}_{s\,cil} \qquad (14)$$

$$K_{s\,plate} = \beta \; K^{*}_{s\,plate} \qquad (15)$$

Fig. 3 shows the evolution of the surface area for the two pore geometries, cylindrical and plates, when β has values of 10 and 100. The surface area is the result of surface generation by calcination and surface losses by sintering. Surface generation, S_{gen}, increases as calcination proceeds until it reaches the value of 104 $m^2\ g^{-1}$ when the particle is totally calcined. Surface loss, S_{loss}, is the decrease in the surface of the particle due to the sintering process. Surface generation depends on the calcination process and, therefore, on those variables that affect the calcination rate such as particle size, temperature and gas bulk concentration. Surface losses depend on the severity of the sintering process, which is dependent on factors such as temperature, sorbent nature, gas composition, etc. The model includes all these factors in the sintering constant, K_S. As can be observed, the pore geometry has an important effect on the surface area of the sorbent. The sorbent with plate-like pores always has higher S values, for the same value of β. And although the initial pore diameter (or pore distance) is the same, it was also observed that the cylindrical pores sinter over a larger area and that the pores have a larger final average diameter than slit pores.

4.2. Determination of the kinetic parameters

The kinetic parameters of the calcination and sintering processes of the various sorbents used here were determined using the model developed and the experimental results were obtained in the drop tube reactor. The corresponding pore geometry of the sorbents was obtained from the adsorption-desorption isotherms so that the appropriate sintering model could be chosen. The model for cylindrical pores was applied to the limestone and the model for slit or plate-like pores to the calcium hydroxides.

The calcination kinetic constants were obtained by fitting the experimental results of calcination conversion, X_C, versus time using the Nelder and Mead method [40] coupled with the model developed. However, this study focused more on predicting the evolution of the pore structure during the residence time of the sorbent in the reactor than on analysing the calcination process, which has been thoroughly studied in the past. To determine the kinetic constants and parameters of the sintering process, the Nelder and Mead method [40] was also used to minimise the squared sum of the differences between the specific surface area predicted by the model and the experimental data. In this way, it was possible to obtain the kinetic parameters of calcination, k_c, and sintering, K_s and S_0, for each temperature and sorbent. The preexponential factors and activation energies for the calcination and sintering processes were later obtained by using the Arrhenius expression with the kinetic data obtained at different temperatures.

The proposed model also made it possible to determine the pore size distribution of the sorbent and its evolution over time, as long as the pore size at which the nascent surface area, S_0, was generated was known. The value of dp_0 was determined by the position of the maximum in the pore size distributions obtained in the experiments at the lowest temperature and shortest reaction time with each sorbent, where the sintering was less important. Because the limestone and the calcium hydroxides had different pore geometries, the data were analysed separately.

4.3. Calcination-sintering of the Omyacarb limestone

Initially, the results obtained during the calcination of the limestone in air at all temperatures and residence times were analysed. It was decided to select a cylindrical pore geometry and a pore diameter of the nascent CaO, dp_0, of 4.3 nm, obtained from pore size distributions with negligible sintering. Fig. 4 shows the evolution of the specific surface area of the Omyacarb limestone at different temperatures, and Fig. 5 shows the evolution of the pore size distribution of the sorbent at 900 °C. The model adequately predicts the evolution of the specific surface area at the different

temperatures, as well as the pore size distribution. The model even predicts the maximum value of S observed at some temperatures, which corresponds to the point at which the sorbent almost reached complete calcination. It must be taken into account that the value of S is the result of surface generation by calcination and surface loss by sintering. Obviously, this maximum appeared earlier as the temperature increased.

The activation energies and the nascent surface area obtained with the proposed method were: E_c=101 kJ mol^{-1}, E_s=69 kJ mol^{-1} and S_0=100 m^2 g^{-1}. Table 3 shows the kinetic parameters obtained with all the sorbents with air and combustion fumes. The value of S_0 obtained here was similar to the 104 m^2 g^{-1} found by Borgwardt [20].

Once the ability of the model to fit the experimental results of the limestone calcination in air had been analysed, the effect of the CO_2 and H_2O concentration in the gas phase on the process was studied. Different percentages of CO_2 between 0 and 15%, and H_2O between 0 and 7%, and mixtures of both gases were used at 1000 °C. The specific surface areas obtained with these gases were considerably smaller than those obtained in air, which demonstrated the important sintering effect of these gases, similar to the results found by other authors [10, 14]. The value of K_s obtained at 1000 °C was strongly dependent on the gas composition, and was fitted to the following empirical equation:

$$K_{s\ (1000\ °C)} = 2.0\ 10^{-10} + 2.6\ 10^{-11}\ \%CO_2 + 5.3\ 10^{-11}\ \%H_2O \qquad (16)$$

Due to the important effect of the CO_2 and H_2O concentration on the sintering process, a reacting gas atmosphere, the composition of which was similar to that of the exhaust gas of a pulverised coal boiler, was selected. It contained 15% CO_2 and 7% H_2O. The calcination parameters in combustion fumes were very similar to those in air (see Table 3) and the fittings were just as good. Recently, Agnew et al. [23] found an activation energy of 99 kJ mol^{-1} for the calcination of the same limestone. This value, very similar to the values reported here, was determined by applying Mai and Edgar's model [12]. However, important differences were found in the kinetic constants of sintering, due to the different decomposition atmospheres. To correctly predict the

experimental data, an initial surface area of 50 m^2g^{-1}had to be used It must be remembered that the initial surface area defined here is not an intrinsic parameter of the sorbent. The difference between this parameter and the nascent surface area of 104 m^2g^{-1} proposed by Borgwardt probably reflects the exponential loss of calcium sites due to thermal sintering in the first 200 ms of reaction [41].

4.4. Calcination-sintering of the calcium hydroxides CH-45 and CH-LGS

The version of the model that assumes plate-like pore geometry was used. The pore diameter of the nascent CaO for the CH45 was of 2.3 nm, obtained from pore size distributions with negligible sintering. However, for the modified calcium hydroxide CH-LGS, two maxima at 2.3 nm and 7.3 nm were obtained in the pore size distribution. For fitting purposes, it was considered that 80% of the surface was generated at 2.3 nm and the rest at 7.3 nm as can be seen from the areas below the curve in the plot. The surface generated at 7.3 nm was considered to be due to the presence of calcium lignosulfonate in the sorbent, a large organic molecule (about 10 nm), which decomposes in boiler conditions to leave big pores.

The kinetic constants, k_c and K_s, and the nascent surface, S_0, were determined for these sorbents (see Table 3). Again, the model predicted the maximum on the surface at different temperatures and that it would appear earlier as temperatures increased. Moreover, the model fitted the experimental pore size distributions: the sintering causes the number of smaller pores to decrease and the number of bigger pores to increase. This is in agreement with the experimental results. The values of K_s found for the hydroxides cannot be directly compared with those found for the limestone because their porous systems are different and the equations used for sintering depend on the pore geometry.

4.5. Comparison of the kinetic parameters obtained for the three sorbents

Fig. 6 compares the experimental and predicted surface areas obtained for the three sorbents at different temperatures and residence times, when the data obtained in a combustion exhaust atmosphere are used. The correlation between the experimental and the predicted values of specific surface areas was quite good.

Fig. 7 shows the values of the kinetic parameters for calcination, k_c, and sintering, K_s, as a function of the temperature in air and in combustion fumes for the three sorbents used. These values were used to obtain the preexponential factors and activation energies given in Table 3. The calcination constant of the limestone was smaller than that of the two calcium hydroxides, which were very similar. Moreover, the reaction atmosphere, air or combustion fumes hardly affected the calcination rate, although the sintering rate dramatically increased in the presence of CO_2 and H_2O. The sintering constants for the limestone and the two hydroxides cannot be directly compared because they have different pore structures and, therefore, a different sintering model was used.

4.6. Comparison with the results obtained by other authors

Previous studies [12,19,44] have shown that the kinetic parameters determined for the decomposition of calcium-based sorbents were greatly dependent on the experimental system and conditions. The activation energies obtained for limestone calcination in a thermogravimetric analyser or in a differential reactor with big particles and temperatures under 900 °C varied between 110 and 204 kJ mol^{-1} [20,42-44]. Moreover, García-Calvo et al. [43] found values that varied between 110 and 194 kJ mol^{-1} depending on the impurity content of the limestone. These values are higher than those obtained in entrained-flow reactors [14, 15, 22], with particles smaller than 100 μm and temperatures as high as 1200 °C, which vary between 33 and 92 kJ mol^{-1}. Mai [11] attributed the higher activation energies obtained to inadequate sorbent/gas mixing or slow particle heat-up. Results were similar for the dehydration of the calcium hydroxide. The activation energies obtained in thermogravimetric analysers or differential reactors

were higher, between 79 kJ mol^{-1} [45] and 280 kJ mol^{-1} [18], than those obtained in a drop tube reactor, which were about 67 kJ mol^{-1} [11, 14].

Therefore, to compare our results with those obtained by other authors, the experimental conditions must be taken into account: particle diameter, temperature window and experimental system. In this study, the estimation of particle heat-up took into account the convection from the bulk gas and reaction wall. The calculations indicated that even the biggest particles (≈50μm) were heated within 8ms of injection. Thus, the activation energy obtained for the calcination of the Omyacarb limestone, 96 kJ mol^{-1}, was similar to that obtained by other authors under similar experimental conditions. However, the values obtained for the CH-45, 36 kJ mol^{-1}, and for the CH-LGS, 50 kJ mol^{-1}, were somewhat lower than those obtained by other authors, although the resistances arising from the different mass transfer processes had been considered in the model.

To validate our model, we compared the results obtained with the sintering models developed by Borgwardt [9] for limestones and by Mai [11] for calcium hydroxide. These models were selected because the experimental conditions used, in terms of particle diameter, residence time and temperature, were in the range of FSI conditions. Fig. 8 shows the evolution of the specific surface area of the sorbent assuming a decomposition atmosphere of nitrogen working at 1000 °C and particle sizes of 50 μm. Our model predicts that results will be similar to those obtained with the Borgwardt and Mai expressions and it also predicts the pore size distribution of the particle and its evolution over time. The most striking aspect of the research was that although our model calculated the total area by adding together the pore sizes in all the layers of the sorbent, the results were very similar to those of other sintering models.

5. Conclusions

A new model to describe the simultaneous processes of calcination and sintering undergone by a calcium sorbent when it is heated at high temperatures is proposed. The model considers cylindrical and plate-like or slit pore geometries. It is able to predict the calcination conversion and the specific surface area in the typical conditions of the sorbent's injection into a pulverised coal boiler. It also predicts the pore size distribution of the sorbent and its evolution over time at different particle locations and in the particle as a whole.

The limestones and calcium hydroxides behaved differently during decomposition and sintering because of their different pore structure and the high initial surface area of the $Ca(OH)_2$. The simulations carried out with the model unequivocally showed that sorbents with cylindrical pores sinter to a greater extent than those with slit pores. The activation energies determined for limestone calcination, 96 kJ mol^{-1}, and for calcium hydroxide dehydration, about 50 kJ mol^{-1}, are in the range of the values found by other authors working in similar experimental conditions.

The reaction atmosphere had a negligible effect on the decomposition kinetic parameters but considerably affected the sintering process. The specific surface areas obtained in atmospheres containing CO_2 and H_2O were lower, by almost 50%, than those obtained under air atmosphere. The increase in sintering when CO_2 and H_2O were present was clearly noticeable in the values of the kinetic parameters obtained for sintering. The value for the initial surface area in combustion fumes was much lower than the one obtained in air atmosphere may be because of an initial exponential loss of surface.

Finally, the proposed model predicted a similar evolution of the specific surface area to that predicted by the equations of various authors working in similar conditions, and it was also able to predict the pore size distribution of the particle and its evolution over time.

Nomenclature

c-CaO	calcium oxide from calcium carbonate
h-CaO	calcium oxide from calcium hydroxide
D_A	molecular diffusion coefficient for CO_2 or H_2O, $m^2\ s^{-1}$
De	effective diffusivity of CO_2 or H_2O in porous lime, $m^2\ s^{-1}$
De_K	effective diffusivity of CO_2 or H_2O in porous lime in the shell K, $m^2\ s^{-1}$
d_i	distance between plates of size i, m
D_{K_i}	Knudsen diffusion coefficient for pores of radius i, $m^2\ s^{-1}$
dp	Particle diameter, m
d_{p0}	characteristic distance of the nascent surface, m
d_{p_i}	pore distance of size i (cylinder radius or distance between plates), m
E_c	activation energy for the calcination process, kJ mol^{-1}
E_S	activation energy for the sintering process, kJ mol-
$fv_{K,i}$	volume fraction of pores of size i in the shell K
fw_K	weight fraction of the shell K
fw_{sorb}	weight fraction of the unreacted core
g(dp)	pore size distribution, $m\ g^{-1}$
k_c^o	pre-exponential factor for the calcination rate, $mol\ m^{-2}\ s^{-1}$
k_C	rate constant for decomposition of the sorbent, $mol\ m^{-2}\ s^{-1}$
k_g	mass transfer coefficient, $m\ s^{-1}$
k_S	rate constant for sintering defined in Eq. (1), s^{-1}, and Eq. (2), $m^{2-2n}\ g^{n-1}\ s^{-1}$
K_S	sintering constant for cylindrical, $g\ m^{-1}\ s^{-1}$, and plates-like, $g\ m^{-2}\ s^{-1}$ geometry
$K_{s_{cil}}$	sintering constant for cylindrical geometry defined in Eq. (14), $g\ m^{-1}\ s^{-1}$
$K_{s_{plate}}$	sintering constant for plate-like geometry defined in Eq. (15), $g\ m^{-2}\ s^{-1}$
K_S^o	preexponential factor for the sintering constant for cylindrical, $g\ m^{-1}\ s^{-1}$, and plate-like, $g\ m^{-2}\ s^{-1}$, geometry
$K_{s_{cil}}^*$	reference basis for sintering constant for cylindrical geometry, $10^{-10}\ gm^{-1}\ s^{-1}$
$K_{s_{plate}}^*$	reference basis for sintering constant for plate-like geometry, $10^{-4}\ g\ m^{-2}\ s^{-1}$
L_i	length of the cylindrical pores of size i, m
M	molecular weight, kg mol^{-1}
n_i	number of pores of characteristic size i
P	partial pressure, atm
P_b	bulk pressure, atm

P_e	equilibrium dissociation pressure of CO_2 or H_2O, atm
R	radius of shrinking core, m
R_g	universal constant of gases, J mol^{-1} K^{-1}
r_i	radius of the cylindrical pores of size i, m
R_p	radius of the particle, m
S	specific surface area, m^2 g^{-1}
S_{ij}	surface area of the pores generated by sintering, m^2 g^{-1}
S_{sorb}	specific surface of the raw sorbent, m^2 g^{-1} CaO
S_0	nascent specific surface area, m^2 g^{-1}
$S_{0K,i}$	initial specific surface area of the shell K, m^2 g^{-1}
S_f	sintered asymptotic specific surface area, m^2 g^{-1}
S_{gen}	specific surface area generated by calcination, m^2 g^{-1}
S_K	specific surface area of the shell K, $m^2 g^{-1}$
$S_{K,i}$	specific surface area of the shell K in pores i, $m^2 g^{-1}$
S_{loss}	specific surface area lost by sintering, m^2 g^{-1}
Sp_i	specific surface of plates of size i, m^2
S_{sorb}	specific surface area of the raw sorbent, m^2 g^{-1}
T	temperature, K
t	time, s
t_c	time for complete calcination, s
z_i	semidistance of plate-like pores of size i, m

Greek letters

β	multiplier factor of the sintering constant
ρ	density, kg m^{-3}
γ	order of sintering
ε_K	porosity of shell K
φ_i	parameters defined in Table 2, m g^{-1}
$\varphi_{K,i}$	parameter φ for pores i in shell K, m g^{-1}
τ	dimensionless time, t / t_c
Ω_i	parameter defined in Table 2, m^2 g^{-1}

Subscripts

i, j, ij	pore sizes
K	number of calcined shell

References

[1] Fukasawa K, Low cost, retrofit FGD systems, IEA Perspectives, London, 1997;34.

[2] Beruto D, Barco L, Searcy AW, Spinolo G. J Am Ceram Soc 1980;63:439.

[3] Gullet BK, Bruce KR. AIChE J 1987;33:1719.

[4] Adánez J, Fierro V, de Diego JA, de Diego F, García-Labiano F. Thermochim Acta 1996;27:151.

[5] Adánez J, Fierro V, García-Labiano F, Palacios JM. Fuel 1997;76:257.

[6] Borgwardt RH, Bruce KR. AIChE J 1986;32:239.

[7] Simons GA, Garman AR. AIChE J 1986;32(9):1491.

[8] Simons GA, Garman A.R. Boni AA. AIChE J 1987;33(2):211.

[9] Borgwardt RH. Chem Engng Sci 1989;44:53.

[10] Borgwardt RH. Ind Engng Chem Res 1989;28:493.

[11] Mai MC. Analysis of simultaneous calcination, sintering and sulphation of calcium hydroxide under furnace sorbent injection conditions. Ph. D. Dissertation. University of Texas, Austin, 1987.

[12] Mai MC, Edgar TF. AIChE J 1989;35(1):30.

[13] German RM., Munir ZA. J Am Ceram Soc 1976;59:379.

[14] Milne CR, Silcox GD, Pershing, DW, Kirchgessner DA. Ind Engng Chem Res 1990;29:139.

[15] Silcox GD, Kramlich JC, Pershing DW. Ind Engng Chem Res 1989;28: 155.

[16] Bruce KR, Gullet BK, Beach LO. AIChE J 1989;35:37.

[17] Adánez J, García-Labiano F, Fierro V. Chem Engng Sci 2000;55:3665.

[18] Irabien A, Viguri JR, Cortabitarte F, Ortiz I. Ind Engng Chem Res 1990;29:1606.

[19] Fuertes AB, Alvarez D, Rubiera F, Pis JJ, Marbán G. Trans IChemEng(A) 1993;71:69.

[20] Borgwardt RH. AIChE J 1985;31:103.

[21] Milne CR, Silcox GD, Pershing DW, Kirchgessner DA. Ind Engng Chem Res 1990;29:2201.

[22] Ghosh-Dastidar A, Mahuli S, Agnihotri R, Fan LS. Chem Engng Sci 1995;50:2029.

[23] Agnew J, Hampartsoumian E, Jones JM, Nimmo W. Fuel 2000;79:1515.

[24] Barret EP, Joyner LG, Halenda PP. J Am Chem Soc 1951;73:373.

[25] Innes WB. Anal Chem 1957; 29:1069.

[26] Powell EK, Searcy AW. Am. Soc. Met. & Met. Soc. of AIME 1980;11B:427.

[27] Hu N, Scaroni AW. Fuel 1996;75(2):177.

[28] Bortz SJ, Roman VP, Yang RJ, Offen GR. Dry Hydroxide Injection At Economiser Temperatures for Improved SO_2 Control. Proc. 1986 Joint Symposium on Dry SO_2 and Simul. SO_2/NO_X Control Technologies, Washington 1986.

[29] Nicholson D. Trans Faraday Society 1965;61:990.

[30] Bortz SJ, Roman, VP, Yang RJ, Offen, GR. Precalcination and its effect on sorbent utilisation during upper furnace injection. Symposium on Dry SO_2/NO_X Control Technologies. Raleigh, North Carolina 1986.

[31] Fuertes AB, Alvárez D, Rubiera F, Pis JJ. Marbán G. Chem Engng Com 1991;109:73.

[32] Al-Shawabkeh A, Matsuda H, Hasatani M. J Chem Engng Japan 1994;27:650.

[33] Mahuli SK, Agnihotri R, Chauk S, Gosh-Dastidar A, Wei SH, Fan LS. AIChE J 1997; 43:2323.

[34] Darroudi T, Searcy AW. J Phys Chem 1981;85:3971.

[35] Weast R. Handbook of chemistry and physics. (48th ed.). Cleveland, OH: CRC Press 1975.

[36] Matsuda H, Ishizu T, Lee SK. Kangaku Kogaku Ronbunshu 1985;11:542.

[37] Satterfield CN. Mass transfer in heterogeneous catalysis, M.I.T. Press, Cambridge, 1970.

[38] Fuller EN, Schettler PD, Giddings JC. Ind Engng Chem 1966;58:19.

[39] Fierro V. Sulphur retention in furnace sorbent injection systems. Ph. D. Dissertation. University of Zaragoza 1998.

[40] Nelder JA, Mead R. Computer J 1964;7:308.

[41] Cole JA, Kramlich JC, Seeker WR, Silcox GD, Newton GH, Harrison DJ, Pershing DW. Fundamental studies on sorbent reactivity in isothermal reactors, Proc. Second Joint Symp. on dry SO_2/NO_X Control Technologies, North Carolina 1986.

[42] Rao TR, Gunn DJ, Bowen JH. Chem Engng Res Des 1989;67:38.

[43] García-Calvo E, Arranz MA, Letón P. Thermochim Acta 1990;170:7.

[44] Khraisha YH, Dugwell DR. Trans. I. Chem. 1991;69:76.

[45] Mu J, Perlmutter DD. Thermochim Acta 1981;49: 207.

Effect of pore geometry on the sintering of Ca-based sorbents during calcination at high temperatures

J. Adánez, V. Fierro and F. García-Labiano

Table 1. Physical properties of calcium-based sorbents

	Limestone	Calcium hydroxides	
	Omyacarb	CH-45	CH-LGS
dp (μm)	45	30	20
S_{sorb} (m^2 g^{-1})	2	19	17
Isotherm (IUPAC)	H1	H3	H3

Table 2. Equations for the sintering model

	Cylindrical pore geometry	Plate-like pore geometry
Characteristic dimension of the new pore ij	$r_{ij} = \left(r_i^2 + r_j^2\right)^{1/2}$	$d_{ij}=d_i+d_j$
Surface area of new pore ij	$S_{ij} = 2\ \pi\ r_{ij}\ L_{ij}$	$Sp_{ij} = \frac{Sp_i + Sp_j}{2} = Sp_i = Sp_j$
Total surface area of pores ij	$S_{ij} = 2\pi\ r_{ij}\ L_{ij}\ n_{ij} = 2\pi\ r_{ij}\ \varphi_{ij}$	$\Omega_{ij} = Sp_{ij}\ n_{ij}$
Disappearance and formation of pores	$d\varphi_{ij} = -d\varphi_i = -d\varphi_j$	$d\Omega_{ij} = - d\Omega_i = - d\Omega_j$
Generation rate of new pores ij	$\frac{d\varphi_{ij}}{dt} = K_s\ \varphi_i\varphi_j$	$\frac{d\Omega_{ij}}{dt} = K_s\ \Omega_i\ \Omega_j$
Surface balance of pores in a single sintering process	$dS_{ij} = 2\pi r_{ij}\ d\varphi_{ij} + 2\pi r_i\ d\varphi_i + 2\pi r_j\ d\varphi_j$	$dS_{ij} = d\Omega_{ij} + d\Omega_i + d\Omega_j$
Variation of surface over time	$\frac{dS}{dt} = \frac{1}{2} 2\pi \sum_{i=1}^{n}\sum_{j=1}^{n}\left[r_{ij}\ d\varphi_{ij} + r_i\ d\varphi_i + r_j\ d\varphi_j\right]$	$\frac{dS}{dt} = \frac{1}{2}\sum_{i=1}^{n}\sum_{j=1}^{n}\ \left[d\Omega_{ij} + d\Omega_i + d\Omega_j\right]$

Table 3 Kinetic parameters for the calcination and sintering processes

	calcination		sintering		
	k_c^o (mol m^{-2} s^{-1})	E_c (kJ mol^{-1})	K_s^o	E_S (kJ mol^{-1})	S_0 (m^2 g^{-1})
air					
limestone	$3.3\ 10^3$	101	$2.5\ 10^{-7}$*	69	100
CH-45	20.4	37	8.8#	74	50
CH-LGS	54.6	48	10.1#	68	50
combustion fumes					
limestone	$2.1\ 10^3$	96	$1.2\ 10^{-6}$*	74	50
CH-45	19.1	36	87.4#	89	50
CH-LGS	53.8	50	49.9#	74	50

* g CaO m^{-1} s^{-1} (cylindrical geometry)

\# g CaO m^{-2} s^{-1} (plate-like geometry)

Captions of the Figures

Fig. 1. Schema of the sintering process for cylindrical and plate-like pores

Fig. 2. a) Evolution over time of the specific surface area profiles along the particle radius, and b) pore size distribution at three locations on the particle radius at τ=1 (k_c=10^{-1} mol m^{-2} s^{-1} and K_s=10^{-9} g m^{-2} CaO s^{-1})

Fig. 3 Effect of the sintering process on the evolution of the specific surface area for two pore geometries (------ S_0-S_{loss}, −··−·· S_{gen})

Fig. 4 Specific surface area evolution of the Omyacarb limestone over time and temperature during its calcination in air (■ experimental, — predicted)

Fig. 5 Evolution of the pore size distribution of the Omyacarb limestone over time during its calcination in air at 900 ºC (● experimental, — predicted)

Fig. 6 Comparison of the experimental and predicted specific surface areas for the three sorbents (● Omyacarb, ▫ CH-45, ■ CH-LGS)

Fig. 7 Comparison of the kinetic and sintering constants for the three sorbents in air and in combustion fumes (● Omyacarb, ▫ CH-45, ■ CH-LGS)

Fig. 8 Comparison of the specific surface areas predicted by the model, and those proposed by Borgwardt [9] for the limestone and Mai [11] for the calcium hydroxide

Effect of pore geometry on the sintering of Ca-based sorbents during calcination at high temperatures

J. Adánez*, V. Fierro, F. García-Labiano

Figure 1

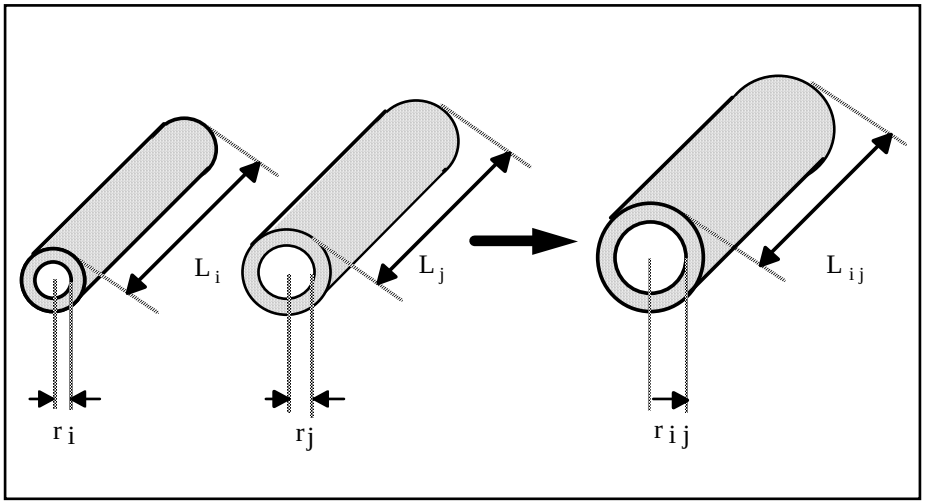

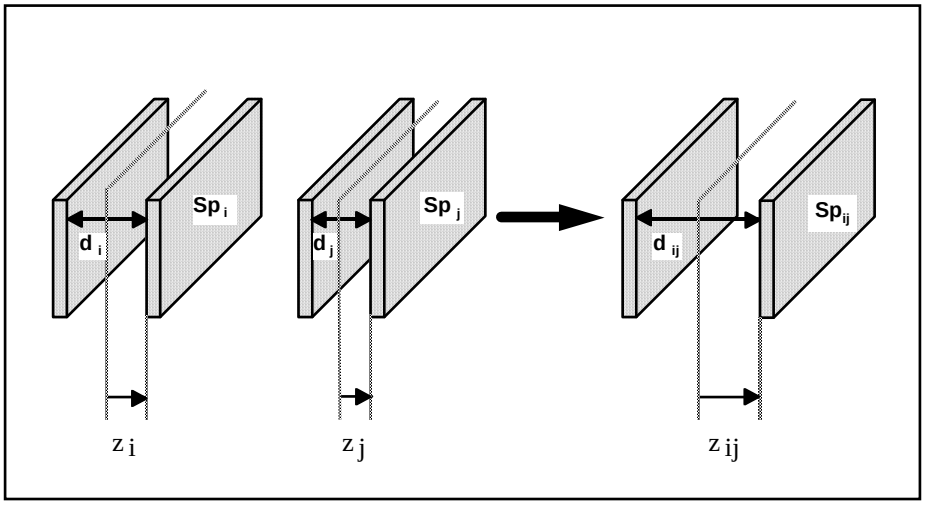

Effect of pore geometry on the sintering of Ca-based sorbents during calcination at high temperatures

J. Adánez*, V. Fierro and F. García-Labiano

Figure 2

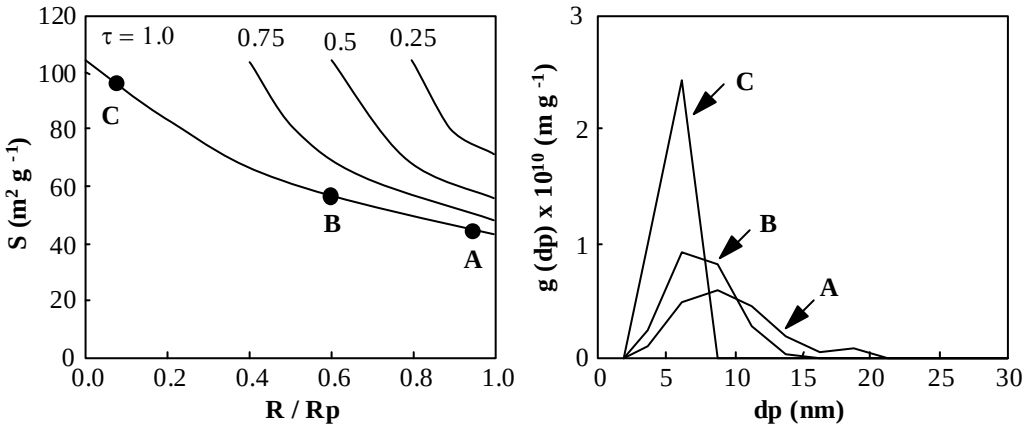

Effect of pore geometry on the sintering of Ca-based sorbents during calcination at high temperatures

J. Adánez*, V. Fierro and F. García-Labiano

Figure 3

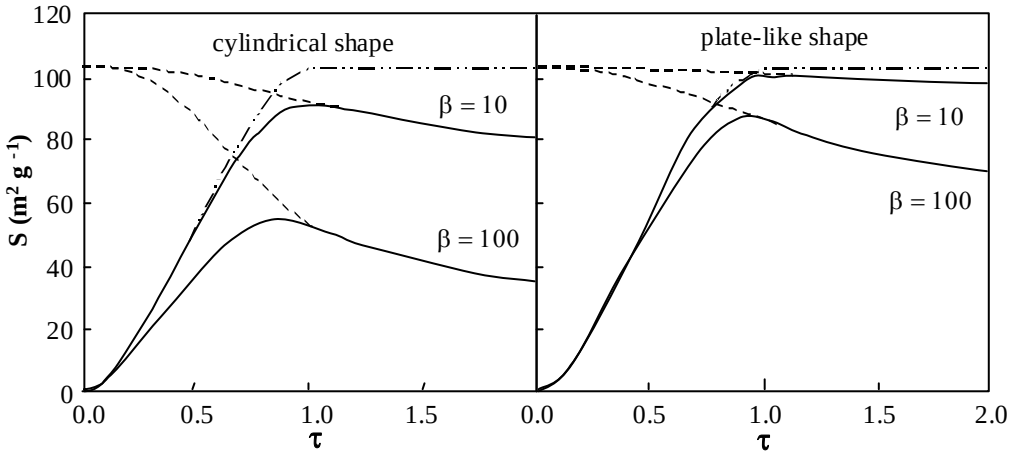

Effect of pore geometry on the sintering of Ca-based sorbents during calcination at high temperatures

J. Adánez*, V. Fierro and F. García-Labiano

Figure 4

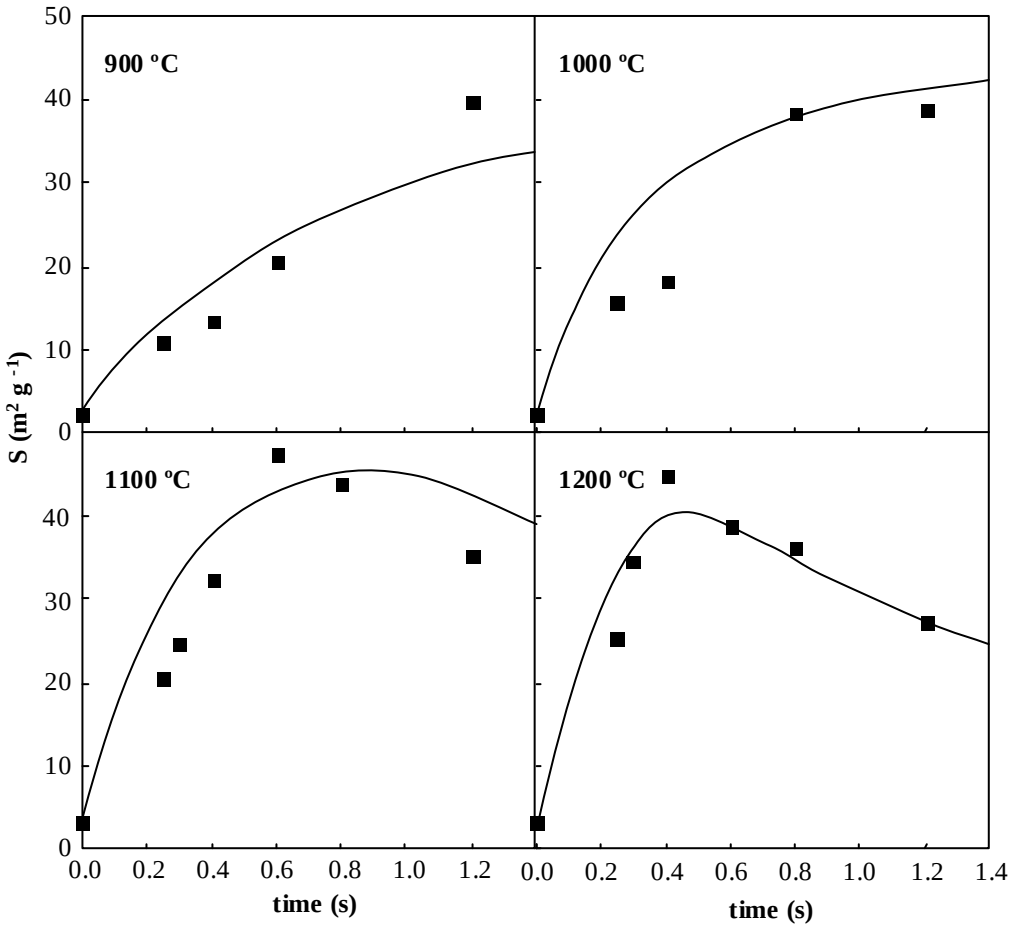

Effect of pore geometry on the sintering of Ca-based sorbents during calcination at high temperatures

J. Adánez*, V. Fierro and F. García-Labiano

Figure 5

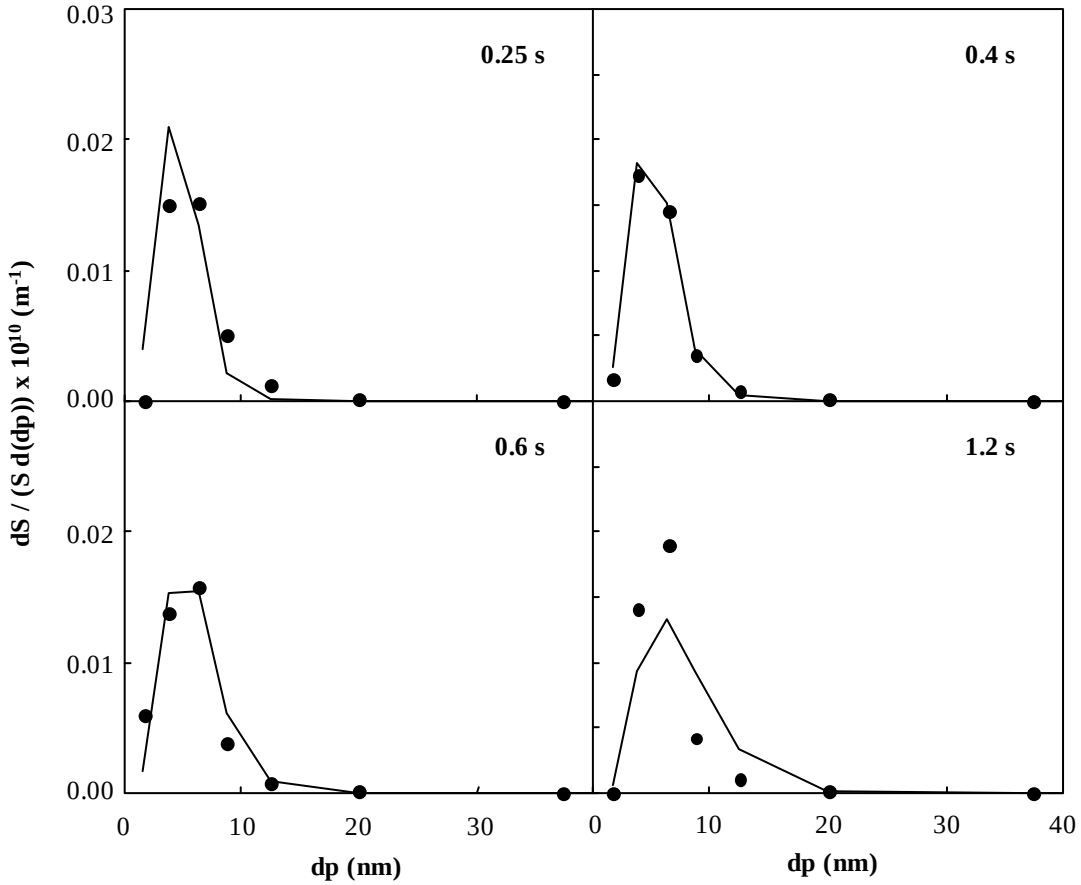

Effect of pore geometry on the sintering of Ca-based sorbents during calcination at high temperatures

J. Adánez*, V. Fierro and F. García-Labiano

Figure 6

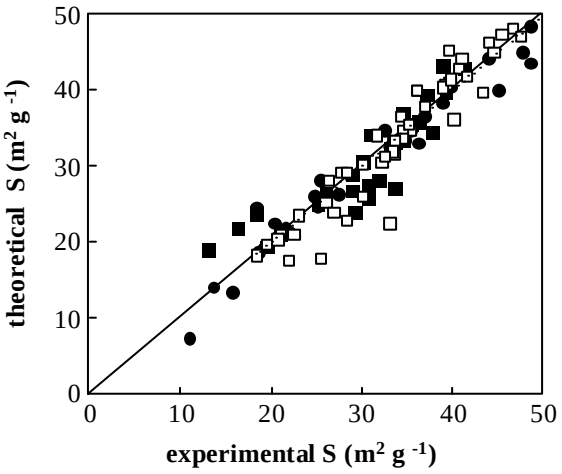

Effect of pore geometry on the sintering of Ca-based sorbents during calcination at high temperatures

J. Adánez*, V. Fierro and F. García-Labiano

Figure 7

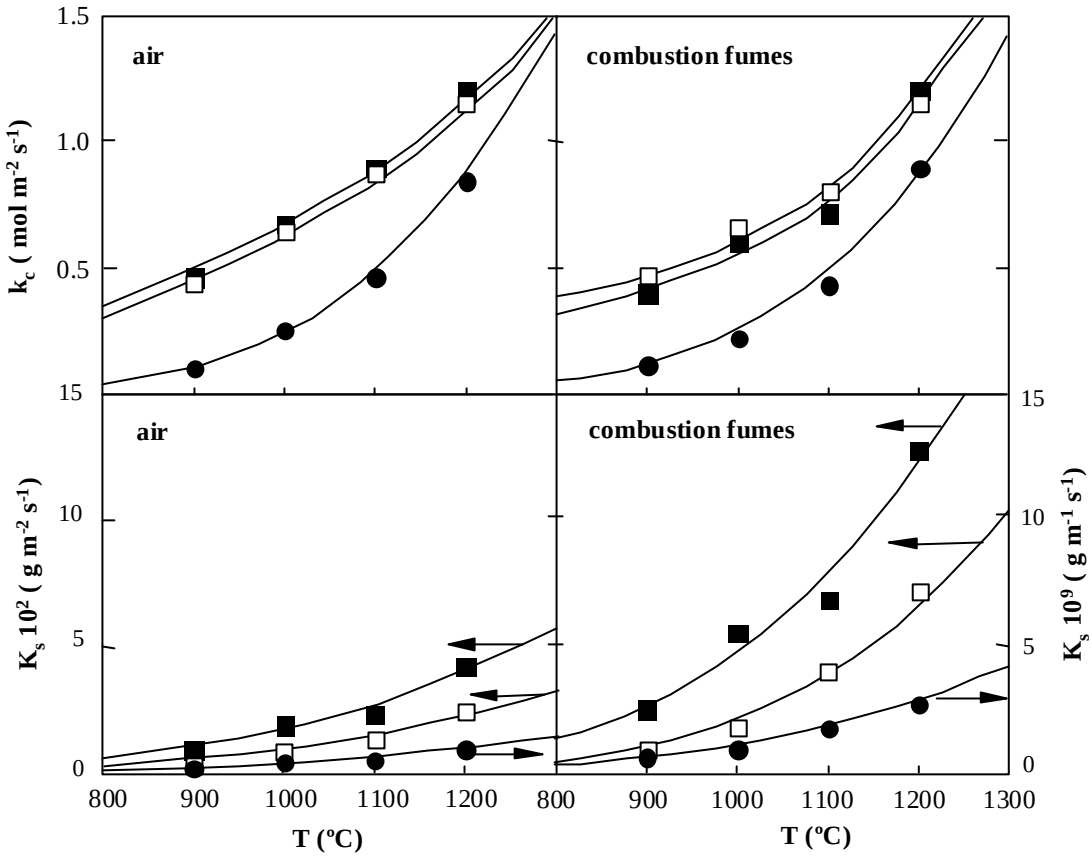

Effect of pore geometry on the sintering of Ca-based sorbents during calcination at high temperatures

J. Adánez*, V. Fierro and F. García-Labiano

Figure 8